

From Single to Multiple Ag-Layer Modification of Au Nanocavity Substrates: A Tunable Probe of the Chemical Surface-Enhanced Raman Scattering Mechanism

Nicolás G. Tognalli,^{†,*} Emiliano Cortés,[‡] Alexander D. Hernández-Nieves,^{†,§} Pilar Carro,[⊥] Gonzalo Usaj,[†] Carlos A. Balseiro,[†] María E. Vela,[‡] Roberto C. Salvarezza,[‡] and Alejandro Fainstein[†]

[†]Centro Atómico Bariloche, Instituto Balseiro, Comisión Nacional de Energía Atómica, 8400 S. C. de Bariloche, Río Negro, Argentina,

[‡]Instituto de Investigaciones Físicoquímicas Teóricas y Aplicadas (INIFTA), Universidad Nacional de La Plata—CONICET,

Sucursal 4 Casilla de Correo 16 (1900) La Plata, Argentina, [§]Departement Fysica, Universiteit Antwerpen, Groenenborgerlaan 171, B-2020 Antwerpen, Belgium, and

[⊥]Departamento de Química Física, Instituto Universitario de Materiales y Nanotecnología, Universidad de La Laguna, Avda. F. Sánchez s/n, 38205-Tenerife, Spain

Surface-enhanced Raman spectroscopy (SERS) combines the capability of molecular fingerprinting with ultrahigh sensitivity, allowing single-molecule detection.¹ Such a combination is unique and cannot be achieved with other spectroscopic techniques. In this way, SERS has given the possibility to study basic chemical and plasmonic phenomena, as well as developing many different analytical applications in various fields such as chemistry, physics, biology, and materials science, among others.^{2–9} Two main different contributions to the SERS enhancement have been identified: the electromagnetic (EM) factor and the so-called chemical contribution. The EM enhancement of SERS-active substrates is mainly determined by the nanostructure of the metallic surface and the wavelength-dependent dielectric properties of the metal. Those properties largely restrict the applicability of SERS to Ag and Au due to their well-behaved optical constants.¹⁰ Beside these standard metals, bimetallic and core–shell surfaces have also been studied as efficient SERS platforms. Different metal partners have been employed in a wide variety of nanostructured surfaces obtained by different physicochemical procedures.^{11–13} Undoubtedly, the Au–Ag bimetallic system is the one studied most, and different strategies have been tested, such as porous-surfaces,¹⁴ mixed Ag(core)/Au(shell) nanoparticles,¹⁵ Ag/Au nanoparticles immobilized on metal

ABSTRACT We present experimental and computational results that enlighten the mechanisms underlying the chemical contribution to surface-enhanced Raman scattering (SERS). Gold void metallic arrays electrochemically covered either by a Ag monolayer or 10–100 Ag layers were modified with a self-assembled monolayer of 4-mercaptopyridine as a molecular Raman probe displaying a rich and unexpected Raman response. A resonant increase of the Raman intensity in the red part of the spectrum is observed that cannot be related to plasmon excitations of the cavity-array. Notably, we find an additional 10–20 time increase of the SERS amplification upon deposition of a single Ag layer on the Au substrate, which is, however, almost quenched upon deposition of 10 atomic layers. Further deposition of 100 atomic Ag layers results in a new increase of the SERS signal, consistent with the improved plasmonic efficiency of Ag bulk-like structures. The SERS response as a function of the Ag layer thickness is analyzed in terms of *ab initio* calculations and a microscopic model for the SERS chemical mechanism based on a resonant charge transfer process between the molecular HOMO state and the Fermi level in the metal surface. We find that a rearrangement of the electronic charge density related to the presence of the Ag monolayer in the Au/Ag/molecule complex causes an increase in the distance between the HOMO center of charge and the metallic image plane that is responsible for the variation of Raman enhancement between the studied substrates. Our results provide a general platform for studying the chemical contribution to SERS, and for enhancing the Raman efficiency of tailored Au-SERS templates through electrochemical modification with Ag films.

KEYWORDS: SERS · chemical effect · nanocavities · UPD · *ab initio*

supports,¹⁶ and core–shell nanoparticle microtubes,¹⁷ among others. Different results have been reported regarding SERS enhancement factors in each particular system.

Despite a lot of work developed regarding bimetallic systems, there are few examples of controlled thickness-layer deposition over a nanostructured-SERS platform. This is probably due to the difficulty

* Address correspondence to tognalli@cab.cnea.gov.ar.

Received for review February 11, 2011 and accepted June 15, 2011.

Published online June 15, 2011
10.1021/nn200567m

© 2011 American Chemical Society

regarding the exact control of thickness in core–shell nanoparticles or porous SERS-active substrates. In this context underpotential deposition (UPD) comes out as the best strategy to deposit exactly one or two layers of a foreign metal on a conducting substrate. Briefly, the UPD phenomenon refers to the electrodeposition of a metal on a foreign metal substrate at potentials that are more positive than those predicted by the Nernst equation for bulk deposition (overpotential deposition, OPD). The UPD process takes place because the deposited adatom–substrate interaction is stronger than the adatom–adatom interaction. The mechanism of UPD has been extensively investigated with various electrochemical and surface characterization techniques.^{18–20} In particular Ag UPD on Au(111) has been taken as a model system for this process. It is well-known that 1 and 2 Ag monolayers are successively deposited on Au at different potential windows.^{21–23} The effect of different UPD monolayers on SERS active metals has been initially explored by Weaver *et al.*,²⁴ finding that UPD Ag and Cu monolayers over rough Au substrates covered with adsorbed halides exhibited only 2 times higher intensity in their SERS spectra than the corresponding plain rough Au. In the same way, quenching in the SERS signal was observed by Pb UPD monolayers on Ag and Cu SERS-active surfaces.²⁵ It has been also reported that only small optical fields exist at the Ag(UPD)–Pt substrate surface which are incapable of supporting the EM enhancement of SERS.²⁶ More recently, it has been shown that the SERS spectra of Rh6G adsorbed on UPD Ag-modified rough Au substrate exhibits a higher intensity when compared with that of Rh6G adsorbed on the Ag-free rough Au.²⁷ In general, the different works in the literature agree with the fact that one UPD monolayer affects SERS intensity at some level. However, quantification of the SERS enhancement factor and a detailed explanation regarding the physicochemical mechanism behind the SERS effect on metal substrates modified by ultrathin metallic layers remain essentially undetermined.

Our approach thus has been to study the SERS response on Au cavity–array substrates extensively investigated by the Bartlett group,^{28–36} modified through a controlled electrochemical deposition of Ag in atomic single and multilayers. Ultrathin silver films on gold templates appear as an attractive strategy that combines the advantages of both metals. Gold is an excellent option for template fabrication, and it is widely used in nanotechnology. Clean and stable nanostructured gold surfaces are relatively simple to prepare. In addition gold hardly forms an oxide layer, and its chemical inertness ensures cleaner surfaces. On the other hand, metallic silver films can be easily deposited on gold by different physical and chemical methods³⁷ in order to get better plasmonic properties of the resulting substrate. Electrodeposition

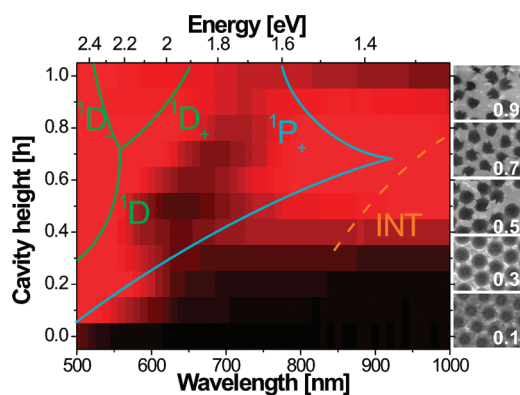


Figure 1. Optical reflectivity intensity map measured with S-polarized light in a $r = 250$ nm Au cavity-array substrate for different void heights. Data were taken with 5 nm steps at 25° incidence angle. The logarithmic color scale describes $R = 0$ with red and $R = 1$ with black. The curves are guides to the eye that identify the different plasmon-polariton modes. The SEM images on the right illustrate the cavity arrays for different h values indicated inside each image.

allows an easy and simple way to modify Au substrates with different Ag amounts ranging from submonolayer/monolayer (UPD) to multilayers (OPD). Here we present a detailed study of the SERS wavelength-dependent response of these nanostructures as a function of void height and Ag-layer thickness. We verify that high-quality Au SERS cavities with thick Ag-layers (~ 30 nm) lead to a Ag bulk-like enhanced SERS response. On the other hand, a relatively thin layer of Ag (~ 3 nm) deposited on the Au-cavities presents a SERS response quite similar to that of bare Au, indicating that the plasmon response is governed by the underlying metal. Notably, we have also observed that deposition of a single-monolayer of Ag leads to significantly enhanced Raman scattering, reaching intensities of the same magnitude or even larger than those recorded on the same substrate covered by bulk Ag and, at some conditions, even 25-folds higher compare to Au nanocavities. An explanation for these results is given based on a study of the molecule–metal substrate interactions based on density-functional *ab initio* calculations and on a theoretical model introduced by Persson to describe the chemical mechanism of SERS enhancement.³⁸ The possibility to modulate an electronic resonant process by metallic single layers is evidenced, providing a detailed description of the parameters involved in this chemical contribution to SERS enhancement.

RESULTS AND DISCUSSION

Experimental Results. We begin this section presenting the plasmonic response of the bare Au cavities. Figure 1 shows the optical reflectivity map of $r = 250$ nm Au cavity arrays as a function of incident wavelength and void height h , defined as a fraction of the void diameter d and ranging from 0 to 1. The

reflectivity (R) is displayed using a logarithmic color scale where red (black) corresponds to the minimum (maximum) value $R = 0$ ($R = 1$). Low reflection values are associated with absorptions and the presence of plasmon modes. The measurements were taken at 25° incidence angle using S-polarized light with wavelengths (λ) covering the range $500 < \lambda < 1000$ nm every 5 nm (horizontal axis). The vertical axis of the map indicates the void-height of the studied graded cavity array. The curves are guides to the eye to identify the optical absorptions assigned to $^1P_+$, 1D_i , $^1D_{+}$, and $^1D_-$ surface plasmon-polaritons. This assignment is based on the Mie plasmon theoretical calculations by T. A. Kelf *et al.*^{30,31} and R. M. Cole *et al.*,³² and described in detail elsewhere.³⁹ The mode noted as INT corresponds to the interaction between plasmon modes belonging to neighbor cavities.³² Note that the reflectivity map does not present plasmonic states in the regions delimited by $600 \leq \lambda \leq 700$ nm and $0.5 \leq h \leq 0.6$ nor for $600 \text{ nm} \leq \lambda$ and $h \leq 0.2$. Reflectivity maps obtained for the Au-cavity substrates modified with 1 and 10 layers of Ag were essentially undistinguishable from the bare Au-structure shown in Figure 1. Upon deposition of bulk-like Ag films (100 layers of Ag), however, notable changes begin to evidence particularly in the green-blue region of the spectra (D Mie-like modes).³⁹ This observation will be useful later to separate the chemical from the electromagnetic SERS contribution.

We now turn to the SERS study of Au cavity-arrays as a function of the surface modification with Ag-coverages using 4-mercaptopyridine (4MP) as a Raman probe, a molecule that yields a similar coverage irrespective of the substrate used as revealed by XPS and reductive desorption curves. We concentrate on the Raman peaks centered around 1100 cm^{-1} shown in Figure 2 for different substrates heights and Ag-layer coverages. Figure 2 presents Raman spectra acquired with green 514.5 nm (top) and red 676.2 nm (bottom) lasers. We have performed Raman measurements using several laser lines, and we find that lasers in the green-blue part of the spectrum are essentially represented by the response observed with 514.5 nm, while the red line (676.2 nm) is representative of what we have also observed at longer wavelengths (650–800 nm). The left and right panels of Figure 2 correspond to the array substrate with voids truncated at $h = 0.2$ (shallow cavities) and $h = 0.6$ (deep cavities), respectively. Raman spectra are presented from bottom to top for substrates with increasing Ag-layer thickness d , ranging from $d = 0$ (bare Au template) to $d \approx 100$ atomic layers. Spectra have been vertically shifted for clarity. We have typically observed somewhat larger backgrounds (presumably originated in residual luminescence) for the UPD-single Ag monolayer on Au, as compared to the rest of the substrates. Several features can be highlighted from the bottom panels of Figure 2. Peaks are observed at 1004

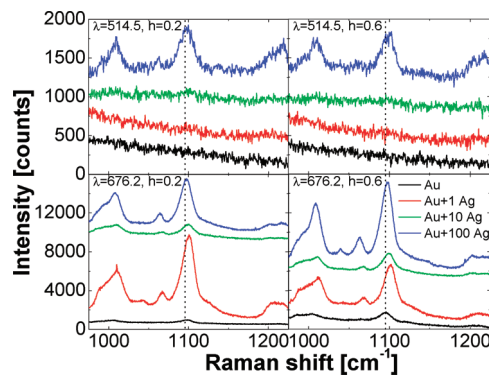


Figure 2. 4MP Raman spectra acquired with green 514.5 nm (top) and red 676.2 nm (bottom) laser light. The panels in the left (right) correspond to the $r = 250$ nm cavity array substrate with voids truncated at $h = 0.2$ ($h = 0.6$). From bottom to top in each panel spectra are presented for substrates with increasing Ag-layer thickness d , ranging from $d = 0$ (bare Au template) to $d = 100$ layers. Spectra have been vertically shifted for clarity.

and 1095 cm^{-1} for 4MP in the bare Au cavity-array. According to published data⁴⁰ these two modes can be assigned to ring C–C stretching vibrations. With only one UPD Ag monolayer deposited on Au, a blue-shift of the modes can be observed reaching 1012 and 1101 cm^{-1} , respectively, and an additional peak can be distinguished at 1068 cm^{-1} . The latter has been assigned to a C–H bending mode.⁴⁰ Upon further deposition of Ag to form the ~ 10 and the ~ 100 atomic layer films, a relative softening of the three 4MP modes toward 1008, 1063, and 1098 cm^{-1} is observed, reaching energies in-between those corresponding to 4MP assembled on the bare Au and UPD Ag substrates. The hardening of the 4MP Raman modes has already been observed when the molecules are self-assembled on bulk Ag, as compared to bulk Au.⁴⁰ On the other hand, the extra blue-shift of the Raman modes for the UPD Ag cavities can be related to the stronger chemical interaction between thiols and UPD Ag reported previously.^{22,23,41,42} Finally, and most importantly, strong variations in the overall peak intensity for the different Ag-coverages and for the two shown void-truncations are evident in Figure 2. We address this central issue next.

For the 514.5 nm excitation almost no signal can be observed with the experimental conditions used for bare Au and the smaller Ag-coverages. Clear SERS signals are however detected with the Ag bulk-like ~ 100 layers deposited film. This can be simply understood in terms of the modified dielectric function of the cavity-arrays when bulk-like ~ 30 nm thick Ag films are grown on the Au-template. For 676.2 nm the behavior is much richer. First, the 4MP spectral features can be already clearly observed for the bare Au cavity-substrates, for both values of void-truncation, $h = 0.2$ and $h = 0.6$. We stress that, as follows from Figure 1, the laser is not resonant with any plasmon mode of the

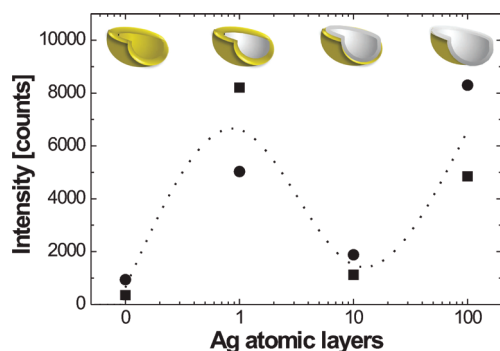


Figure 3. Raman intensity corresponding to the 4MP $\approx 1100 \text{ cm}^{-1}$ mode as a function of the number of Ag atomic layers deposited on $h = 0.2$ (squares) and $h = 0.6$ (circles) Au cavities measured using the 676.2 nm laser line. The dashed line is a guide to the eye to emphasize the overall behavior described in the text. The inset shows a representation of the Au cavities with different Ag coverages.

cavities. Thus, the observed behavior could only be partially understood by consideration of the plasmon modes determined by the dielectric properties of Au. In fact, the observed behavior could be related to a non-resonant coupling of the 676.2 nm laser line with the $^1P_+$ plasmon for $h = 0.2$ and with the $^1P_+$ and 1D plasmon modes for $h = 0.6$.⁴³ Second, and most notably, a very strong enhancement of the Raman intensity is observed upon deposition of a *single* layer of Ag atoms for the two shown void-heights and is particularly noticeable for $h = 0.2$. The observed signal amplification amounts to about 20 for $h = 0.2$, and 6 for $h = 0.6$. Third, this latter Raman enhancement is quenched upon further deposition of Ag until the ~ 10 layer film is formed. Finally, a clear SERS amplification is recovered when the Ag deposited is thick enough to form a bulk-like coverage. Figure 3 summarizes the above results presenting the $\sim 1100 \text{ cm}^{-1}$ Raman mode intensity as a function of the number of Ag layers for the cavity arrays with voids of thickness $h = 0.2$ (squares) and $h = 0.6$ (circles), measured using the 676.2 nm laser line. It is clearly observed how the Raman signal increases when an UPD Ag monolayer is deposited, followed by a signal reduction when ~ 10 Ag layers are reached, and a final intensity growth for the thick Ag-coverage. This SERS increase for the thicker Ag-coverage is fully compatible with what is observed with the 514.5 nm laser and can be understood on the basis of the extra electromagnetic SERS enhancement caused by the appearance of bulk Ag plasmons when the film thickness equals ~ 100 layers ($\sim 30 \text{ nm}$). This is a clear demonstration of the potentiality of the reported strategy to make Ag-like substrates based on high-quality ordered Au-templates. What remains to be explained, and we address in what follows, is the notable and anomalous amplification of the SERS signal observed at 676.2 nm in the UPD Ag-covered substrates, and its disappearance when ~ 10 layers of Ag ($\sim 3 \text{ nm}$ thick film) are grown on gold. We recall that both XPS and reductive desorption

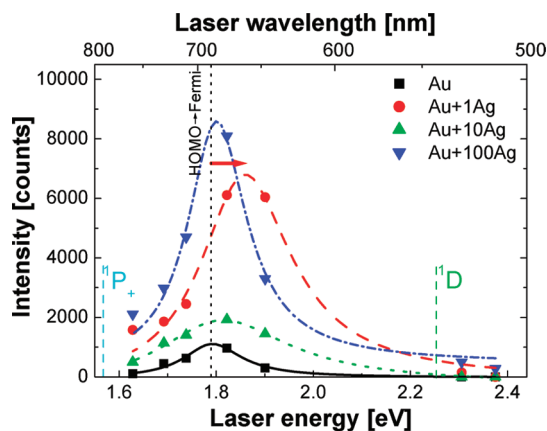


Figure 4. Raman intensity scans corresponding to the 4MP $\approx 1100 \text{ cm}^{-1}$ mode as a function of the incident laser energy for the $h = 0.6$ Au cavity modified with four different Ag film thicknesses ($d = 0$, squares; $d = 1$, circles; $d \approx 10$, up triangles; and $d \approx 100$ layers, down triangles). The lines are Lorentzian fits shown as guides to the eye. The vertical dashed lines indicate the position of the $^1P_+$ and 1D plasmons while the dotted lines highlight the molecule-to-metal charge transfer resonance.

experiments performed on the complete set of samples show the same 4MP coverage independently of the Ag film thickness.

In Figure 4 we present Raman intensity scans for the 4MP $\approx 1100 \text{ cm}^{-1}$ mode as a function of the incident laser for different Ag thicknesses deposited on the Au cavity. We chose to show the $h = 0.6$ Au cavity substrate to minimize the influence of the nanostructure plasmons on the intensity scan response within the used laser range ($514.5 < \lambda < 770 \text{ nm}$). The purpose is to decouple the chemical from the electromagnetic responses as a function of the Ag film thickness d (see Figure 1). Essentially the same behavior is observed for $h = 0.2$. The square dots represent the measured intensities for Au cavities, while circles, triangles, and inverted triangles correspond to the intensities measured on 1, ~ 10 , and ~ 100 layers of Ag on Au cavities, respectively. The shown lines are Lorentzian fits presented as guides to the eyes. We highlight three important features in these results. First, there is a clear Raman resonance at 650–700 nm, an energy range where no plasmon modes are present for any of the cavity-arrays independently of the Ag coverage (see Figure 1 and ref 39). In fact, the wavelength of these maxima are far from both $^1P_+$ and 1D plasmon resonances at $h = 0.6$, and even further from the 4MP molecular HOMO-to-LUMO optical absorption which is around 330 nm (see Supporting Information). Second, the qualitative Raman intensity behavior with increasing Ag thicknesses along the whole laser range is in agreement with the single wavelength data presented in Figure 3. This is evidence that this peculiar latter phenomena is essentially wavelength independent within the described spectral range. Third, while all the scans present their maxima around the laser line $\lambda = 676.2 \text{ nm}$, there is small but notable relative

blue-shift of the Raman resonance maximum for the Ag monolayer film (indicated with an arrow in Figure 4). All the observations reported up to this point strongly indicate a new optical resonance for all substrates (nonexistent in the separate individual molecules or in the bare cavity-arrays), and the presence of additional changes in the electronic interaction on the Au/UPD-Ag/4MP complex as compared to both the Au/4MP and Au/OPD-Ag/4MP systems. These kind of optical resonances and electronic changes related to variations in Raman intensities are typically identified in the literature as SERS *chemical mechanisms*.⁴⁴

An important result that needs to be addressed within this scenario, and before we pass to a more quantitative analysis, is the observed decrease in the Raman intensity for the ~ 10 Ag layer film. On one hand, when ~ 10 Ag atomic layers are deposited on Au, the 4MP molecule is now attached to a Ag atom that presents its electronic structure unaltered with respect to bulk Ag (the influence of the electronic properties of Au are almost completely screened by the ~ 10 layers of Ag). The latter is supported by the Raman mode shift observed in Figure 2, which is similar to that measured for 4MP on ~ 100 layers of Ag. On the other hand, the plasmonic response should be quite similar to that of the Au substrate because the light penetration depth on Ag (around 30 nm) is larger than the film thickness for ~ 10 layers of Ag (~ 3 nm). This results in a light–plasmon interaction governed by the underlying (weaker respect to Ag) Au response. According to these considerations, for the cavity substrate covered with ~ 10 Ag layers the additional electronic modification proposed to be acting on the molecule–substrate interaction in UPD-Ag would not be present, nor is the bulk Ag electromagnetic SERS amplification due to the reduced film thickness and the consequent absence of well-defined Ag plasmons. These two added effects explain qualitatively the SERS intensity reduction for the ~ 10 layers Ag film.

Theoretical results. Summarizing, we evidence the existence of two different Raman amplification regimes depending of the Ag coverage: (i) a regime mainly described by an additional *chemical* mechanism appearing with a single Ag atomic layer, which acts on top of the plasmonic SERS response of Au, and (ii) a regime mainly determined by the improved electromagnetic plasmon response of bulk Ag, which can be eventually accompanied by a smaller chemical contribution of 4MP in Ag.⁴⁵ The latter Ag-plasmonic regime is operative when the Ag-film is thick compared to the light penetration depth (~ 100 Ag layers). Coexistent with both regimes there is clear evidence of the presence of a new Raman resonance intrinsically related to the electronic structure of 4MP bound to the metal surface. Hereafter we will focus our effort to explain the *chemical* regime. Notwithstanding this conceptual identification with a chemical mechanism, we

note that the microscopic understanding of the latter is still under strong debate.^{38,46–48} Several models have been put forward depending on the specific system under study, including the adatom,⁴⁶ the metal–molecule charge transfer resonance,³⁸ and the polarizability modulation^{47,48} models, among several others. On the basis of our experimental results we will base our discussion in a model proposed by Persson³⁸ and characterized by charge transfer excitations between the molecule and the metal. This model grasps many of the basic components of various other proposed chemical mechanisms and, in addition, allows for a quantitative evaluation of the SERS response through the following expression for the differential Raman scattering cross section:³⁸

$$\frac{d\sigma}{d\Omega} = \frac{4\omega'^4}{3c^4} (ed)^4 |\varepsilon_a'(0) G(\omega, \omega')|^2 |\langle n=1|Q|n=0\rangle|^2 \quad (1)$$

Here, e is the electron charge, d is an effective distance, included in the model to account for the change of the electrostatic potential between the position of the center of charge of the orbital $|a\rangle$ and the image plane given by the metallic surface, $\varepsilon_a'(0)$ is the first derivative of the energy of the orbital $|a\rangle$ with respect to the displacement coordinate Q , $G(\omega, \omega')$ is an integrate expression depending on the incident and scattered photons ω and ω' , and $\langle n=1|Q|n=0\rangle$ is the matrix element of the displacement operator Q between the vibrational ground state $|n=0\rangle$ and the first vibrational excited state $|n=1\rangle$.⁴⁹ We see from eq 1 that the Raman cross section is thus essentially determined by three concurring contributions, namely (i) the magnitude by which a specific vibrational mode modulates the molecular electronic states (given by $\varepsilon_a'(0)$), (ii) the resonant terms involving the laser and scattered photons, and the transitions between molecular and metallic electronic levels (given by $G(\omega, \omega')$), and finally (iii) the molecule-to-image-plane effective distance (given by d). This latter term comes into play as a consequence of the additional energy that is required to transfer an electron from the molecule to the metal (or vice versa) due to the screening charges generated at the metal surface.

To provide quantitative estimation for these different factors involved in the Raman cross section of the Persson model eq 1, we have performed DFT *ab initio* calculations of the electronic states, molecule-on-surface structure, and vibrational energies, for the different studied Ag-modified Au-substrates. These calculations were done considering (111) unreconstructed metallic substrates, a 4MP monolayer in $\sqrt{3} \times \sqrt{3}$ R30° configuration (coverage $1/3$), and taking into account periodic boundary conditions. We note that neither experimental nor theoretical agreement exists about the Au(111)^{50,51} and Ag(111)^{52–54} reconstructions induced by thiol adsorption. We have

TABLE 1. Adsorption Energies in eV for a $1/3$ coverage of 4MP Monolayer Assembled in a $\sqrt{3} \times \sqrt{3}$ R30° Lattice on Different (111) Substrates

substrate	up-right	bridge tilted
Au	−1.35	−1.41
Au+1Ag	−1.87	−1.78
Ag	−1.70	−1.62

selected a $\sqrt{3} \times \sqrt{3}$ R30° configuration for modeling our systems on the basis of the thermodynamic calculations of the surface free energy between different reported lattices for these systems.^{55,56} This fact also allows for an easier comparison between the different substrates. The molecule adsorption configuration for each substrate was found by energy relaxation calculations. The result, shown in Table 1, is that 4MP adsorbs in a bridge-position slightly shifted to the fcc site and tilted 27° (bfcc) with respect to the substrate normal for Au(111), while acquiring an upright configuration on both fcc UPD and OPD Ag surfaces (ufcc).

In Figure 5 we present the electronic density-of-states (DOS) as a function of energy calculated for three important model cases as a function of the metallic composition: Au/4MP (top), Au/UPD-Ag/4MP (center), and Ag/4MP (bottom). The calculation for 4MP bound to “bulk” Ag is intended to model the electronic structure of both the Au+10Ag and Au+100Ag samples. The Fermi level is defined as the 0 eV state. In each panel both the total DOS (black lines) and the molecule projected DOS (gray lines) are drawn. Different contributions to the DOS are present that change as the film composition varies. We observe intense low energy structures (less than −2 eV for Au, less than −3 eV for Ag) arising mainly from contributions of the electronic d-states of the metallic film. The shift of the edge of these structures from *ca.* −2 eV for Au to *ca.* −3 eV for the bulk Ag film, is the origin of the reddish and white color of each metal. We note in both the total and partial molecular DOS a well-defined peak centered around *ca.* −1.25 eV for the Au film substrate (indicated with a dotted line). This peak corresponds to the highest occupied molecular orbital (HOMO). Notably, it moves toward *ca.* −1.4 eV for the Au/UPD-Ag film and shifts back to *ca.* −1.3 eV when the Ag film is used as a substrate. This shift of the HOMO level is a strong indication that the molecular response is sensitive to the film composition, and in particular to the electronic state of the metallic surfaces. This result is in qualitative agreement with the experimental behavior of the maxima of the Raman intensity scans presented in Figure 4, where a blue shift from 1.8 to 1.9 eV is also observed for the UPD Ag substrate. This correlation supports the identification of the HOMO-to-Fermi charge transfer transition in the involved Raman resonance mechanism. The ~ 0.5 eV energy difference between experiments and calculations could be due

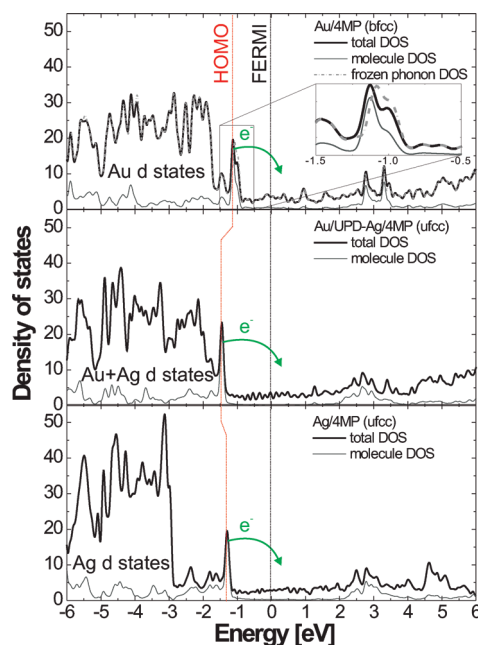
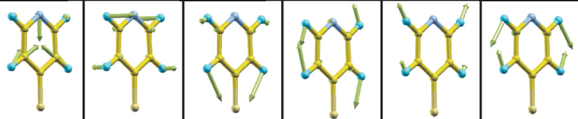


Figure 5. Density-of-states (DOS) based on *ab initio* calculations performed for 4MP molecules adsorbed on three different fcc (111) surfaces: Au (top panel), Au/UPD-Ag (center panel), and Ag (bottom panel). Note that 4MP is adsorbed in a bridge tilted configuration for the Au substrate (bfcc) and in a upright one for the other two metallic films (ufcc). Black lines represent the total DOS. The gray lines describe the DOS projected on the molecular states. The dotted vertical line indicates the position of the molecular HOMO state for the different substrates. The arrows represent the molecule to metal electronic transition. The inset shows the HOMO shift (dashed line) when a frozen phonon calculation is performed, see text for details.

to the specific metal surface reconstruction. Similar energy shifts have been observed in other systems,⁵⁷ but such detailed study is out of the scope of this paper. Finally, we also see in both total and partial DOS a group of peaks between 2.5 and 3.5 eV that can be assigned to the lowest unoccupied molecular orbital (LUMO). Note that the HOMO–LUMO or the metal–LUMO charge transfer resonances are also possible candidates for the observed Raman resonance. However, the calculated values for these transitions, $E_{\text{HOMO}} - E_{\text{LUMO}} \geq 3.5$ eV, and $E_{\text{Fermi}} - E_{\text{LUMO}} \geq 2.5$ eV are well above the experimentally observed resonance, even when *ab initio* calculations typically underestimate the energy of excited states.

Table 2 presents a comparison between the experimentally measured and computationally calculated vibrational frequencies for the 4MP adsorbed on the metal surfaces. The measured frequencies corresponding to the four studied substrates are presented in the top panel (Exp.). What can be observed is the hardening of the 4MP modes when the substrate changes from Au to Au+1Ag, followed by a softening of the frequencies to intermediate values when 10 and 100 layers of Ag are grown on Au (Au+10Ag, Au+100Ag), as previously described in Figure 2. In the bottom panel

TABLE 2.^a

	sample	shoulder	v. i. peak	peak	i. peak	v. i. peak	peak	peak
Exp.	Au	987	1005	-	1065	1098.5	-	1212
	Au+1Ag	988	1010	1042	1067	1101	1205	1217
	Au+10Ag	984	1009	1042	1066	1099.5	1203	1215.5
	Au+100Ag	983	1008	1042	1064.5	1098	1201.5	1216
Calc.	Au (bfcc)	978	992	1059	1071	1076	-	1215
	free 4MP	967	971	1049	1068	1079	1202	-
	free 4MP							

^a Top panel (Exp.): measured frequencies in cm^{-1} corresponding to the four studied systems: Au, Au+1Ag, Au+10Ag, and Au+100Ag. The first line indicates the observed intensity for each vibrational mode. Bottom panel (Calc.): *ab initio* calculated vibrational modes for both the bridge tilted 4MP on fcc Au and the free 4MP together with the corresponding graphical representations of the atom displacements within each mode.

(Calc.) we present the *ab initio* calculated vibrational modes for both the bridge-tilted 4MP on Au(111) and the free 4MP molecule. We find a quite good agreement with the experimental results within a 2% numerical uncertainty. At the bottom of the figure we represent the different atom displacements corresponding to each one of the presented vibrational modes for the free 4MP. Notwithstanding the excellent agreement between experimental and calculated vibrational frequencies, we note that this 2% is larger than the experimental variations observed for the different studied substrates. We have thus not intended an *ab initio* evaluation of these substrate-dependent behavior.

Besides allowing for a proper assignment of the observed vibrational frequencies, the above results are important because they allow the identification of the relevant molecular orbital in our system ($|a\rangle$ in Persson's model) through a frozen phonon DOS calculation. These calculations involve the evaluation of the system's total energy for an out of equilibrium configuration characterized by the displacement of the molecular atoms according to a given vibrational eigenvector. In the inset of the top panel of Figure 5 we illustrate the effect of such a frozen phonon displacement on the DOS calculation using the most intense $\sim 992 \text{ cm}^{-1}$ vibrational mode for the Au/4MP system. The most noticeable change in the DOS appears in the HOMO state, which shifts 0.05 eV toward higher energies (see inset of Figure 5). These results evidence those electronic levels that are more strongly modified by the vibrational states, thus contributing most through $\epsilon_a'(0)$ in eq 1 to the chemical resonance mechanism. On the basis of the previously presented experimental results and on these *ab initio* calculations we thus identify the HOMO molecular state as the $|a\rangle$ molecular orbital involved in the molecule-to-metal charge

transfer transition of the chemical resonant SERS process. These transitions occur from the HOMO state to above the Fermi level, as indicated with arrows in Figure 5.

Having identified the HOMO as the molecular orbital involved in Persson's description, we proceed to determine the distance d for the different substrates (see eq 1). This has been accomplished by integrating the DOS of Figure 5 for each one of the modeled substrates in the regions of the HOMO (-1.6 to -1.0 eV) and the metallic (0 to 0.4 eV) states. The latter, which are the states involved in the charge transfer mechanism, are also representative of the local density of states around the Fermi energy. This is a good approximation to the electrostatic response of the metallic surface. As a result, we present in Figure 6 the charge density projected on the corresponding atoms for the HOMO (left column) and Fermi states (right column) for the three different systems: Au/4MP (top panel), Au/UPD-Ag/4MP (center panel), and Ag/4MP (bottom panel). It follows that the HOMO charge density is centered in the 4MP molecule, with a small contribution from the metallic substrates. This last contribution appears because the total DOS is summed, that is, the molecule and the metallic contribution. Note that the contribution of the Au atoms is bigger than the one of Ag because of the larger spectral overlap between HOMO and metallic d states. A higher charge density is also observed for "bulk" Au in the last atomic layer of the metal as compared with the rest of substrate atoms, consistent with an hybridization between the molecule and the metal surface atoms. On the other hand, we observe that the Fermi states are mainly localized on the substrate atoms, even when an hybridization with the 4MP S atom is also present. The most noteworthy result, however, is the fact that there appears almost no charge density at the Ag atoms in the Au/UPD-Ag

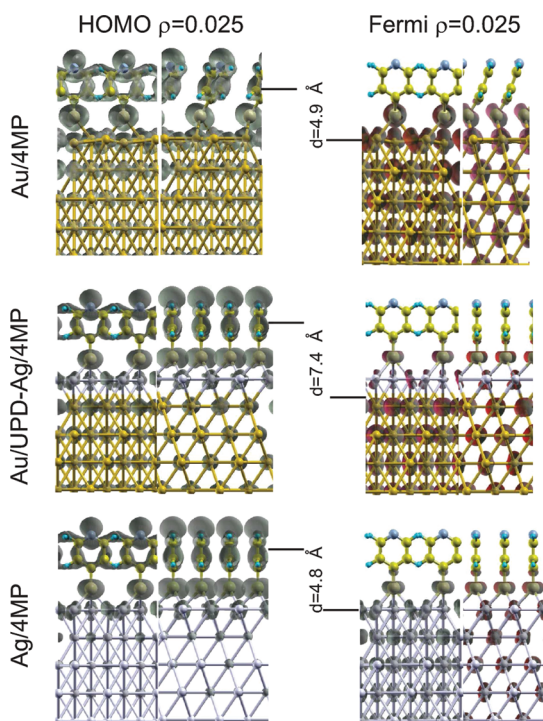


Figure 6. Projected charge density for the three different substrates Au/4MP (top), Au/UPD-Ag/4MP (center), and Ag/4MP (bottom) corresponding to the HOMO state (left column) and the states close to the Fermi energy (right column) obtained from the integration of the DOS of Figure 5 in the -1.6 to -1.0 eV and 0 to 0.4 eV ranges, respectively. The d values shown in the central column represent the effective distances used in our model for each system.

substrate. We note that this effect is also supported by Pauling's electronegativities which for Au and Ag are 2.3 and 1.8 eV, respectively.^{58,59} It is also consistent with the work function values we have calculated for Au(111), Au(111)/UPD-Ag, and Ag(111), without adsorbate, which are 5.23, 5.24, and 4.54 eV, respectively. The absence of charge density in the UPD-Ag atoms results in an increase of d (a shift of the image plane) with respect to the other metallic substrates. In the central column of Figure 6 we give this effective distance for each of the studied systems. We estimate d as a charge weighted distance average between the 4MP S and N atoms to the last Au and Ag atomic layers in the Au and Ag substrates, respectively, and to the last two atomic layers in the Au/UPD-Ag substrate. Comparing the obtained d values we can clearly observe an increment in d for the Au/UPD-Ag substrate respect to the Au and Ag "bulk-like" versions. Recalling from eq 1 that the Raman cross section depends on the 4th power of d , we can indeed expect an important Raman signal enhancement for the Au/UPD-Ag substrate arising from this contribution.

Summarizing our analysis of the model presented in eq 1 we expect an important contribution from the $G(\omega, \omega')$ term.³⁸ In addition, the role of d has also been shown to be important (see Figure 6). On the other hand, we have not observed any evidence of variations

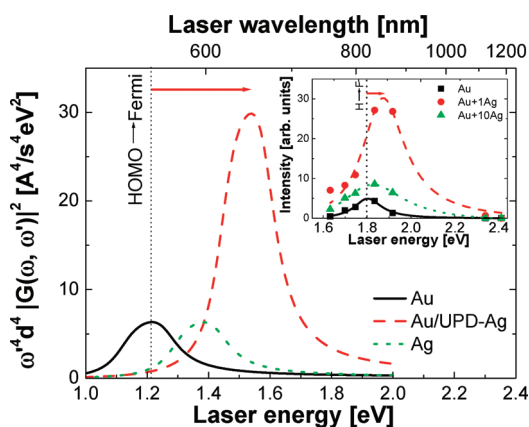


Figure 7. $|\omega'^2 d^2 G(\omega, \omega')|^2$ factor as a function of ω for each one of the three different systems: Au/4MP (full line), Au/UPD-Ag/4MP (dashed line), and Ag/4MP (dotted line). The involved parameters were obtained from *ab initio* DFT calculations (for more details see the Supporting Information and the discussion in the text). The inset shows the experimentally measured Raman resonant scan for the Au, Au+1Ag, and Au+10 substrates modified with a 4MP monolayer.

of $\epsilon_a'(0)$ in the different studied substrates. Our calculations also show that this factor could depend on the specific surface reconstruction under consideration, the determination of which is out of our present scope. We thus modeled the Raman cross section as proportional to $|\omega'^2 d^2 G(\omega, \omega')|^2$ using as input data for $\rho_a(\epsilon)$ and d the parameters arising from the *ab initio* calculations of Figures 5 and 6, respectively. In Figure 7 we present $|\omega'^2 d^2 G(\omega, \omega')|^2$ as a function of ω for each one of the three different systems: Au/4MP (full line), Au/UPD-Ag/4MP (dashed line), and Ag/4MP (dotted line). We recall that the calculation performed for Ag/4MP is conceived to model the chemical contribution for both the Au+10Ag and the Au+100Ag SERS substrates. However, the latter also presents, as already discussed, an extra electromagnetic contribution due to the presence of bulk Ag plasmons. We consequently compare the chemical mechanism calculations in Figure 7 with the experimental resonant Raman scans obtained only for Au, Au+1Ag, and Au+10Ag (shown in the inset of Figure 7). The model reproduces notably well the measured intensity ratios and the relative shift of the Raman resonance scan maxima. As commented before, there exists an energy mismatch of ~ 0.4 eV which is probably due to an inaccurate energy position of the calculated HOMO state presumably caused by the real surface reconstruction effects which were not taken into account in the DOS calculations. Nevertheless, it is clear that the results provide strong evidence for the applicability of Persson's model of chemical enhancement with the microscopic contributions obtained from *ab initio* calculations. We find that the most important contribution to the chemical enhancement mechanism in the studied system is the existence of a new molecule-Fermi level charge transfer resonance

with, in addition, a novel effect due to the shift of the image plane observed on the Au/UPD-Ag substrate. This results in a very important and easy way to chemically enhance the Raman signal of molecules by depositing an UPD Ag atomic layer on Au nanocavities. While these results have been demonstrated specifically for 4MP and for the studied cavity-arrays, the calculations indicate that the main conclusions should be of more general applicability to many different molecules bound to UPD Ag-modified Au plasmonic substrates.

CONCLUSIONS

We have presented a detailed SERS investigation of $r = 250$ nm Au-nanocavity templates modified by the controlled electrochemical deposition of Ag from 1 to 100 atomic layers using UPD and OPD techniques. We have analyzed their structural properties and their wavelength dependent plasmon and SERS responses as a function of the number of deposited Ag layers. A significant increase of the SERS amplification in the red part of the spectrum is observed for all substrates with, in addition, a relative amplification amounting to 5–20 being observed for the UPD-modified substrates. This

augmented response has been analyzed in terms of *ab initio* calculations and a microscopic model for the SERS chemical mechanism which involves a molecule-to-Fermi level charge transfer transition. We find that a rearrangement of the electronic charge density related to the presence of the Ag monolayer in the Au/UPD–Ag/molecule complex causes an increase in the distance between the HOMO center of charge and the metallic image plane which is responsible for the relative Raman enhancement of this substrate. This signal enhancement is quenched upon further deposition of 10 layers of Ag due to the changes in the OPD Ag electronic structure. Further deposition of Ag to achieve 100 atomic layers of Ag-modified Au substrate results in a new increase of the SERS signal both in the red and the green part of the spectrum, compatible with a Ag bulk-like structure and a consequent more efficient electromagnetic contribution to the signal enhancement. The reported results provide a general platform for enhancing the response of plasmonic substrates by UPD-modification and provide deep insight on the basic mechanisms underlying the so-called chemical enhancement in SERS processes.

METHODS

Substrate Fabrication. The nanovoid arrays have been fabricated *via* an hexagonal close packed self-assembly of 250 nm radius (r) polystyrene spheres, followed by an electrochemical Au deposition, as originally described by Bartlett and co-workers.^{28–36} Ultrathin Ag films were electrochemically deposited on the Au templates from 5×10^{-4} M $\text{Ag}_2\text{SO}_4 + 1$ M H_2SO_4 aqueous solution in a conventional electrochemical cell using a Pt large area foil as counter electrode and a Ag wire as reference electrode. The electrodeposition was made at a constant potential in the underpotential regime (UPD) to form a complete monolayer (ML) and in the overpotential range (OPD) to form ~ 10 and ~ 100 layers. The Au and the Ag-covered Au templates were modified with a self-assembled monolayer of 4-mercaptopyridine (for more details regarding sample preparation procedures see the Supporting Information.).

Optical Measurements. The reflectivity measurements were performed using a fully automated Wollam WVASE32 variable angle spectroscopic ellipsometer with focusing probes that give a 100 μm circular spot on the sample, and sustain a numerical aperture of 0.02. The SERS measurements were performed on the metallic nanocavities modified with a close-packed monolayer of self-assembled 4MP molecules, chosen because of the nonresonant Raman response of the free molecule in the used laser spectral range. The Raman scattering experiments were performed on a Jobin-Yvon T64000 triple spectrometer operating in subtractive mode and equipped with a liquid N_2 cooled charge coupled device (CCD). The excitation was done using various lines of an Ar–Kr laser (specifically 514.5, 530, 647.1, and 676.2 nm), and a Ti-Sapphire laser continuously tunable between 690 and 1080 nm. Measurements were performed on dry samples with freshly prepared 4MP monolayers. Spectra were acquired in parallel S-polarization for 10 s using 20 mW of laser power with incidence angle of 25° and focused on a circular spot of 30 μm diameter. The collection numerical aperture was 0.2, aligned normal to the surface. The reported data are the result of three complete repetitions of series of experiments performed with the $r = 250$ nm graded Au array-cavity substrates. In all cases we tested the bare Au and the three studied Ag-coverages, probing eight

void heights ranging from $h = 0.1$ to $h = 0.9$, including in addition a flat Au substrate, and using different laser wavelengths.

Calculations. The *ab initio* calculations were performed using density functional theory. The surface was modeled by a periodic slab composed of five metal layers and a vacuum of ~ 12 Å (similar qualitative results were obtained for three metal layers). Molecule adsorption occurs only on one side of the slab. During the geometry optimization the two bottom layers were kept fixed at their optimized bulk truncated geometry. The three outermost atomic metal layers as well as the atomic coordinates of the adsorbed species were allowed to relax without further constraints. The atomic positions were relaxed until the force on the unconstrained atoms was less than 0.02 eV/Å. The tolerance used to define self-consistency was 10^{-5} eV for the single-point total energy and 10^{-4} eV for the geometry optimization. The unit cell employed in all calculations was a ($\sqrt{3} \times \sqrt{3}$) of the Au(111) or Ag(111) surfaces. The calculations were performed with the Quantum Espresso⁶⁰ and the VASP 4.6^{61,62} packages, and we obtained an excellent agreement between them (see the Supporting Information for details regarding the Quantum Espresso and VASP calculations).

Acknowledgment. We acknowledge financial support from ANPCyT (Argentina, PICT08-1617, PICT08-2236, PICT06-621, PICT-CNPQ-08-0019, PAE 22711, PICT06-01061, PICT06-483) and Project CTQ2008-06017/BQU, Spain. N.G.T., E.C., A.D.H.N., R.C.S., G.U., C.A.B., and A.F. are also at CONICET. M.E.V. is a member of the research career of CIC BsAs. R.C.S., C.A.B., and A.F. are Guggenheim Foundation Fellows. We would like to thank Dr. M. H. Fonticelli for fruitful discussions on the electrochemical measurements and Dr. H. Pastoriza for the help with the SEM measurements.

Supporting Information Available: Substrate fabrication; calculations; details of the Persson's model. This material is available free of charge *via* the Internet at <http://pubs.acs.org>.

REFERENCES AND NOTES

1. Le Ru, E. C.; Meyer, M.; Etchegoin, P. Proof of Single-Molecule Sensitivity in Surface Enhanced Raman Scattering

- (SERS) by Means of a Two-Analyte Technique. *J. Phys. Chem. B* **2006**, *110*, 1944–1948.
- Etchegoin, P.; Maher, R. C.; Cohen, L. F.; Hartigan, H.; Brown, R. J. C.; Milton, M. J. T.; Gallop, J. C. New Limits in Ultrasensitive Trace Detection by Surface Enhanced Raman Scattering (SERS). *Chem. Phys. Lett.* **2003**, *375*, 84–90.
 - Freeman, R. G.; Grabar, K. C.; Allison, K. J.; Bright, R. M.; Davis, J. A.; Guthrie, A. P.; Hommer, M. B.; Jackson, M. A.; Smith, P. C.; Walter, D. G.; *et al.* Self-Assembled Metal Colloid Monolayers: An Approach to SERS Substrates. *Science* **1995**, *267*, 1629–1632.
 - Tognalli, N.; Fainstein, A.; Calvo, E.; Bonazzola, C.; Pietrasanta, L.; Campoy-Quiles, M.; Etchegoin, P. SERS in PAH-Os and Gold Nanoparticle Self-Assembled Multilayers. *J. Chem. Phys.* **2005**, *123*, 044707–1/9.
 - Kiely, C. J.; Fink, J.; Brust, M.; Bethell, D.; Schiffrin, D. J. Spontaneous Ordering of Bimodal Ensembles of Nanoscopic Gold Clusters. *Nature* **1998**, *396*, 444–446.
 - Félidj, N.; Aubard, J.; Lévi, G.; Krenn, J. R.; Salerno, M.; Schider, G.; Lamprecht, B.; Leitner, A.; Aussenegg, F. R. Controlling the Optical Response of Regular Arrays of Gold Particles for Surface-Enhanced Raman Scattering. *Phys. Rev. B* **2002**, *65*, 075419–1/9.
 - Jackson, J. B.; Westcott, S. L.; Hirsch, L. R.; West, J. L.; Halas, N. J. Controlling the Surface-Enhanced Raman Effect via the Nanoshell Geometry. *Appl. Phys. Lett.* **2003**, *82*, 257–259.
 - Kelly, K. L.; Coronado, E.; Zhao, L. L.; Schatz, G. C. The Optical Properties of Metal Nanoparticles: The Influence of Size, Shape, and Dielectric Environment. *J. Phys. Chem. B* **2003**, *107*, 668–677.
 - Dick, L. A.; McFarland, A. D.; Haynes, C. L.; Van Duyne, R. P. Metal Film over Nanosphere (MFON) Electrodes for Surface-Enhanced Raman Spectroscopy (SERS): Improvements in Surface Nanostructure Stability and Suppression of Irreversible Loss. *J. Phys. Chem. B* **2002**, *106*, 853–860.
 - Le Ru, E. C.; Etchegoin, P. G. *Principles of Surface Enhanced Raman Spectroscopy and Related Plasmonic Effects*; Elsevier: Amsterdam, The Netherlands, 2008.
 - Andrade, G. F. S.; Brolo, A. G.; Temperini, M. L. A. Comparison of SERS Performances of Co and Ni Ultrathin Films over Silver to Electrochemically Activated Co and Ni Electrodes. *J. Phys. Chem. C* **2008**, *112*, 15348–15355.
 - Wang, Y.; Song, W.; Ruan, W.; Yang, J.; Zhao, B.; Lombardi, J. R. SERS Spectroscopy Used To Study an Adsorbate on a Nanoscale Thin Film of CuO Coated with Ag. *J. Phys. Chem. C* **2009**, *113*, 8065–8069.
 - Ji, N.; Ruan, W.; Wang, C.; Lu, Z.; Zhao, B. Fabrication of Silver Decorated Anodic Aluminum Oxide Substrate and Its Optical Properties on Surface-Enhanced Raman Scattering and Thin Film Interference. *Langmuir* **2009**, *25*, 11869–11873.
 - Lu, L.; Eychmüller, A. Ordered Macroporous Bimetallic Nanostructures: Design, Characterization, and Applications. *Acc. Chem. Res.* **2008**, *41*, 244–253.
 - Cui, Y.; Ren, B.; Yao, J.; Gu, R.; Tian, Z. Synthesis of AgcoreAushell Bimetallic Nanoparticles for Immunoassay Based on Surface-Enhanced Raman Spectroscopy. *J. Phys. Chem. B* **2006**, *110*, 4002–4006.
 - Driskell, J. D.; Lipert, R. J.; Porter, M. D. Labeled Gold Nanoparticles Immobilized at Smooth Metallic Substrates: Systematic Investigation of Surface Plasmon Resonance and Surface-Enhanced Raman Scattering. *J. Phys. Chem. B* **2006**, *110*, 17444–17451.
 - Wang, T.; Hu, X.; Dong, S. A Renewable SERS Substrate Prepared by Cyclic Depositing and Stripping of Silver Shells on Gold Nanoparticle Microtubes. *Small* **2008**, *4*, 781–786.
 - Borissov, D.; Aravinda, C. L.; Freyland, W. J. Comparative Investigation of Underpotential Deposition of Ag from Aqueous and Ionic Electrolytes: An Electrochemical and *In Situ* STM Study. *Phys. Chem. B* **2005**, *109*, 11606.
 - Esplandiú, M. J.; Schneeweiss, M. A.; Kolb, D. M. An *In Situ* Scanning Tunneling Microscopy Study of Ag Electrodeposition on Au(111). *Phys. Chem. Chem. Phys.* **1999**, *1*, 4847.
 - Rooryck, V.; Reniers, F.; Buess-Herman, C.; Attard, G. A.; Yang, X. The Silver UPD on Gold(111) Revisited. *J. Electroanal. Chem.* **2000**, *482*, 93.
 - Ogaki, K.; Itaya, K. *In Situ* Scanning Tunneling Microscopy of Underpotential and Bulk Deposition of Silver on Gold (111). *Electrochim. Acta* **1995**, *40*, 1249.
 - Fonticelli, M. H.; Benitez, G.; Carro, P.; Azzaroni, O.; Salvarezza, R. C.; Gonzalez, S.; Torres, D.; Illas, F. Effect of Ag Adatoms on High-Coverage Alkanethiolate Adsorption on Au(111). *J. Phys. Chem. C* **2008**, *112*, 4557–4563.
 - Jennings, G. K.; Laibinis, P. E. Underpotentially Deposited Metal Layers of Silver Provide Enhanced Stability to Self-Assembled Alkanethiol Monolayers on Gold. *Langmuir* **1996**, *12*, 6173–6175.
 - Leung, L. W. H.; Gosztola, D.; Weaver, M. J. Surface-Enhanced Raman Scattering From Gold Electrodes Modified by Underpotential-Deposited Silver and Copper Monolayers: Spectral and Double-Layer Comparisons with Silver and Copper Electrodes. *Langmuir* **1987**, *3*, 45–52.
 - Ingram, J. C.; Pemberton, J. E. Investigation of the Quenching of Surface Enhanced Raman Scattering from Pyridine on Copper and Silver Electrodes by Underpotential Deposition of Lead. *Langmuir* **1992**, *8*, 2040–2048.
 - Miragliotta, J.; Furtak, T. E. Enhanced Raman Scattering with One Monolayer of Silver. *Phys. Rev. B* **1987**, *35*, 7382–7391.
 - Liu, Y.; Yang, K.; Hsu, T. Enhancements in Intensity and Thermal Stability of Raman Spectra Based on Roughened Gold Substrates Modified by Underpotential Deposition of Silver. *J. Raman Spectrosc.* **2009**, *40*, 903–907.
 - Bartlett, P. N.; Birkin, P. R.; Ghanem, M. A. Electrochemical Deposition of Macroporous Platinum, Palladium and Cobalt Films Using Polystyrene Latex Sphere Templates. *Chem. Commun.* **2000**, 1671–1672.
 - Coyle, S.; Netti, M. C.; Baumberg, J. J.; Ghanem, M. A.; Birkin, P. R.; Bartlett, P. N.; Whittaker, D. M. Confined Plasmons in Metallic Nanocavities. *Phys. Rev. Lett.* **2001**, *87*, 176801–1/4.
 - Kelf, T. A.; Sugawara, Y.; Baumberg, J. J.; Abdelsalam, M. E.; Bartlett, P. N. Plasmonic Band Gaps and Trapped Plasmons on Nanostructured Metal Surfaces. *Phys. Rev. Lett.* **2005**, *95*, 116802–1/4.
 - Kelf, T. A.; Sugawara, Y.; Cole, R. M.; Baumberg, J. J.; Abdelsalam, M. E.; Cintra, S.; Mahajan, S.; Russell, A. E.; Bartlett, P. N. Localized and Delocalized Plasmons in Metallic Nanovoids. *Phys. Rev. B* **2006**, *74*, 245415–1/12.
 - Cole, R. M.; Baumberg, J. J.; García de Abajo, F. J.; Mahajan, S.; Abdelsalam, M. E.; Bartlett, P. N. Understanding Plasmons in Nanoscale Voids. *Nano Lett.* **2007**, *7*, 2094–2100.
 - Teperik, T. V.; Popov, V. V.; García de Abajo, F. J.; Abdelsalam, M.; Bartlett, P. N.; Kelf, T. A.; Sugawara, Y.; Baumberg, J. J. Strong Coupling of Light to Flat Metals via a Buried Nanovoid Lattice: The Interplay of Localized and Free Plasmons. *Optics Express* **2006**, *14*, 1965–1972.
 - Lacharmoise, P. D.; Tognalli, N. G.; Goñi, A. R.; Alonso, M. I.; Fainstein, A.; Cole, R. M.; Baumberg, J. J.; García de Abajo, F. J.; Bartlett, P. N. Imaging Optical Near Fields at Metallic Nanoscale Voids. *Phys. Rev. B* **2008**, *78*, 125410–1/5.
 - Baumberg, J. J.; Kelf, T. A.; Sugawara, Y.; Cintra, S.; Abdelsalam, M. E.; Bartlett, P. N.; Russell, A. Angle-Resolved Surface-Enhanced Raman Scattering on Metallic Nanostructured Plasmonic Crystals. *Nano Lett.* **2005**, *5*, 2262–2267.
 - Cintra, S. H.; Abdelsalam, M. E.; Bartlett, P. N.; Baumberg, J. J.; Kelf, T. A.; Sugawara, Y.; Russell, A. E. Sculpted Substrates for SERS. *Faraday Discuss.* **2006**, *132*, 191–200.
 - Salvarezza, R. C.; Arvia, A. J. In *Modern Aspects of Electrochemistry*; Bockris, J.O'M., White, R. E., Eds.; Plenum Press: New York, 1996; Vol. 28, pp 289–367.
 - Persson, B. N. J. On the Theory of Surface-Enhanced Raman Scattering. *Chem. Phys. Lett.* **1981**, *82*, 561–565.
 - Cortés, E.; Tognalli, N.; Fainstein, A.; Vela, M. E.; Salvarezza, R. C. Ag-Modified Au Nanocavity SERS Substrates. *Phys. Chem. Chem. Phys.* **2009**, *11*, 7469–7475.

40. Orendoff, C. J.; Gearheart, L.; Jane, N. R.; Murphy, C. O. Aspect Ratio Dependence on Surface Enhanced Raman Scattering Using Silver and Gold Nanorod Substrates. *Phys. Chem. Chem. Phys.* **2006**, *8*, 165–170.
41. Fonticelli, M.; Azzaroni, O.; Benitez, G.; Martins, M. E.; Carro, P.; Salvarezza, R. C. Molecular Self-Assembly on Ultrathin Metallic Surfaces: Alkanethiolate Monolayers on Ag(1 × 1)-Au(111). *J. Phys. Chem. B* **2004**, *108*, 1898–1905.
42. Azzaroni, O.; Vela, M. E.; Andreasen, G.; Carro, P.; Salvarezza, R. C. Electrodesorption Potentials of Self-Assembled Alkanethiolate Monolayers on Ag(111) and Au(111). An Electrochemical, Scanning Tunneling Microscopy and Density Functional Theory Study. *J. Phys. Chem. B* **2002**, *106*, 12267–12273.
43. Note that the 514.5 nm line is also close to resonance with the $^1P_+$ and 1D plasmons for $h = 0.2$ and $h = 0.6$, respectively. However, as it is well established the large electronic interband absorption present in Au strongly quenches the Raman enhancement in the green-blue part of the spectra.¹⁰
44. Moskovits, M. Surface-Enhanced Spectroscopy. *Rev. Mod. Phys.* **1985**, *57*, 783–826.
45. Shegai, T.; Vaskevich, A.; Rubinstein, I.; Haran, G. Raman Spectroelectrochemistry of Molecules within Individual Electromagnetic Hot Spots. *J. Am. Chem. Soc.* **2009**, *131*, 14390–14398.
46. Otto, A.; Timper, J.; Billman, G.; Kovacs, G.; Pockrand, I. Surface Roughness Induced Electronic Raman Scattering. *Surf. Sci.* **1980**, *92*, L55.
47. Persson, B. N. J.; Zhao, K.; Zhang, Z. Chemical Contribution to Surface-Enhanced Raman Scattering. *Phys. Rev. Lett.* **2006**, *96*, 207401–1/4.
48. Otto, A. The Chemical (Electronic) Contribution to Surface-Enhanced Raman Scattering. *J. Raman Spectrosc.* **2005**, *36*, 497–509.
49. See the Supporting Information for more details on the Persson's model.
50. Vericat, C.; Vela, M. E.; Benitez, G.; Carro, P.; Salvarezza, R. C. Self-Assembled Monolayers of Thiols and Dithiols on Gold: New Challenges for a Well-known System. *Chem. Soc. Rev.* **2010**, *39*, 1805–1834.
51. Rissner, F.; Egger, D. A.; Romaner, L.; Heimel, G.; Zojer, E. The Electronic Structure of Mixed Self-Assembled Monolayers. *ACS Nano* **2010**, *4*, 6735–6746.
52. Yu, M.; Woodruff, D. P.; Bovet, N.; Satterley, C. J.; Lovelock, K.; Jones, R. G.; Dhanak, V. Structure Investigation of Ag-(111)($\sqrt{7} \times \sqrt{7}$)R19°-SCH₃ by X-ray Standing Waves: A Case of Thiol-Induced Substrate Reconstruction. *J. Phys. Chem. B* **2006**, *110*, 2164–2170.
53. Torres, D.; Carro, P.; Salvarezza, R. C.; Illas, F. Evidence for the Formation of Different Energetically Similar Atomic Structures in Ag(111)-($\sqrt{7} \times \sqrt{7}$)R19°-SCH₃. *Phys. Rev. Lett.* **2006**, *97*, 226103.
54. Yu, M.; Woodruff, D. P.; Satterley, C. J.; Jones, R. G.; Dhanak, V. Structure of the Pentythiolate Self-Assembled Monolayer on Ag(111). *J. Phys. Chem. C* **2007**, *111*, 10040–10048.
55. Keith, J. A.; Jacob, T. Theoretical Studies of Pd Metal Deposition on the $\sqrt{3} \times \sqrt{3}$ 4-Mercaptopyridine Self-Assembled Monolayer. *Electrochim. Acta* **2010**, *55*, 8258–8262.
56. We have also performed calculations on 4MP monolayer in $\sqrt{7} \times \sqrt{7}$ R19° configuration for Au(111)/UPD-Ag and Ag(111) unreconstructed surfaces (as another common configuration used for thiol adsorption on Ag surfaces). Our calculations indicate through the obtained surface free energy that the $\sqrt{3} \times \sqrt{3}$ R30° is a more stable configuration for 4MP monolayer on Au(111)/UPD-Ag and Ag(111).
57. Carro, P.; Corthey, G.; Rubert, A. A.; Benitez, G. A.; Fonticelli, M. H.; Salvarezza, R. C. The Complex Thiol-Palladium Interface: A Theoretical and Experimental Study. *Langmuir* **2010**, *26*, 14655–14662.
58. Kolb, D. M.; Gerischer, H. Further Aspects Concerning the Correlation between Underpotential Deposition and Work Function Differences. *Surf. Sci.* **1975**, *51*, 323–327.
59. Gordy, W.; Orville Thomas, W. J. Electronegativities of the Elements. *J. Chem. Phys.* **1956**, *24*, 439–444.
60. Giannozzi, P.; Baroni, S.; Bonini, N.; Calandra, M.; Car, R.; Cavazzoni, C.; Ceresoli, D.; Chiarotti, G. L.; Cococcioni, M.; Dabo, I.; *et al.* QUANTUM ESPRESSO: A Modular and Open-Source Software Project for Quantum Simulations of Materials. *J. Phys.: Condens. Matter* **2009**, *21*, 395502, <http://www.quantum-espresso.org>.
61. Kresse, G.; Joubert, D. From Ultrasoft Pseudopotentials to the Projector Augmented-Wave Method. *Phys. Rev. B* **1998**, *59*, 1758–1775.
62. Kresse, G. Furthmüller, Efficient Iterative Schemes for *ab-initio* Total-Energy Calculations Using a Plane-Wave Basis Set. *Phys. Rev. B* **1996**, *54*, 11169–11185.